SIAM J. SCI. COMPUT.
Vol. 19, No. 6, pp. 1958–1979, November 1998
© 1998 Society for Industrial and Applied Mathematics
010

FIRST-ORDER SYSTEM LEAST SQUARES (FOSLS) FOR CONVECTION-DIFFUSION PROBLEMS: NUMERICAL RESULTS*

J. M. FIARD†, T. A. MANTEUFFEL†, AND S. F. MCCORMICK†

Abstract. The focus of this paper is on planar linear convection-diffusion problems, to which we apply a special form of first-order system least squares (FOSLS [Cai et al., *SIAM J. Numer. Anal.*, 31 (1994), pp. 1785–1799; Cai, Manteuffel, and McCormick, *SIAM J. Numer. Anal.*, 34 (1997), pp. 425–454]). This we do by introducing the gradient of the primary variable, scaled by certain exponential functions. The convection-diffusion equation is then recast as a minimization principle for a functional corresponding to a sum of weighted L^2 norms of the resulting first-order system. Discretization is accomplished by a Rayleigh–Ritz method based on standard finite element subspaces, and the resulting linear systems are solved by basic multigrid algorithms. The main goal here is to obtain optimal discretization accuracy and solver speed that is essentially uniform in the size of convection. Our results show that the FOSLS approach achieves this goal in general when the performance is measured either by the functional or by an equivalent weighted H^1 norm. Included in our study is a multilevel adaptive refinement method based on locally uniform composite grids and local error estimates based on the functional itself.

Key words. least squares, multigrid, convection-diffusion

AMS subject classifications. 65F10, 65N20

PII. S1064827596301169

1. Introduction.

Convection-domimated equations are some of the more difficult problems to solve numerically. Linear convection-diffusion equations arise, for example, in the modeling of fluid flow based on Fick's law and in the linearization of the incompressible Navier–Stokes equations. Classical numerical methods, such as centered finite differences or standard Galerkin finite elements, are generally unsuitable for such problems, because they become unstable—and therefore produce overly oscillatory solutions—when the perturbation parameter (i.e., relative size of diffusion) tends to zero. Mixed methods [1, 3, 13, 17] have also been applied with limited success. It is well known that upwind-type strategies, including upwind finite volume [11] and artificial streamline diffusion [12] methods, can restore stability, but this is usually at the sacrifice of accuracy. Methods that exhibit performance results that are uniform in the perturbation parameter include the Petrov–Galerkin techniques described in [10] and [14]. These methods are based on the use of exponential test and trial functions. The consistency results presented in [14] were motivated by the numerical results documented in [10], which studied and compared several different Petrov–Galerkin methods on variable coefficient separable problems. The method in [10] that showed the best performance was proved in [14] to be globally convergent and first-order accurate in the discrete L^2 norm, uniformly in the perturbation parameter.

In an attempt to obtain stronger results (uniform accuracy and convergence in a scaled H^1 norm), we focus here on first-order system least-squares methods (FOSLS) [5, 6]. The FOSLS methodology consists of recasting the second-order convection-diffusion equation (by introducing, in our case, vector flux as a new variable) into a

*Received by the editors March 21, 1996; accepted for publication (in revised form) February 4, 1997; published electronically July 27, 1998. This work was sponsored by the French Foreign Office grant Lavoisier, the Air Force Office of Scientific Research grant AFOSR-91-0156, the National Science Foundation grant DMS-8704169, and the Department of Energy grant DE-FG03-93ER25165.
http://www.siam.org/journals/sisc/19-6/30116.html

†Department of Applied Mathematics, Campus Box 526, University of Colorado at Boulder, Boulder, CO 80309-0526 (tmanteuf@boulder.colorado.edu, stevem@newton.colorado.edu).

first-order system, which is then used to formulate a least-squares functional. The basis of our work is the theory in [6] that establishes equivalence between the bilinear part of the FOSLS functional and the square of the vector H^1 norm, with the attendant approximation properties of the Rayleigh–Ritz discretization method and convergence properties of multigrid techniques. We summarize these results tailored to our specific convection-diffusion problem in the following section.

Unfortunately, these basic estimates depend critically on the perturbation parameter, and they degrade in the convection-dominated regime. To counter this dependence, we develop a new FOSLS approach that involves a careful rescaling of the functional by exponential terms. The bilinear part of this new functional exhibits equivalence to an associated scaled vector H^1 norm uniformly in the perturbation parameter, with attendant uniform and optimal discretization accuracy and solver speed. One important aspect of this FOSLS approach is that all variables (the original scalar variable and its gradient) are computed accurately (uniformly so) in an H^1-like norm. Thus, for example, the derivatives of the error are controlled and spurious oscillations are avoided. We report on several tests that demonstrate such uniform finite element discretization accuracy as well as multigrid solver efficiency.

We must emphasize that the results obtained here are stronger than those obtained in [10], for example, in the sense of the stronger H^1 norm. In fact, our estimates are uniform in an L^2 norm as well as an H^1 norm and for the flux as well as the primitive variable. However, our norms incorporate a scaling that has the effect of dramatically changing the influence of the boundary layer. On the other hand, the estimates in [10] are uniform in the standard L^2 norm, which incorporates no such scaling.

An additional benefit of FOSLS is that the functional is zero at the exact solution, so it automatically provides a sharp a posteriori measure of the error. We will exploit this feature by using individual element contributions to the functional in a simple adaptive strategy to determine where to refine. Our results show that such a scheme can produce grids that are properly tailored to the solution.

2. FOSLS.

2.1. Problem formulation.

Assume that Ω is a bounded, open, connected domain in $\mathbf{R}^2$ with Lipschitz boundary $\partial\Omega = \Gamma_D \cup \Gamma_N$. Our focus is the planar linear convection-diffusion problem

$$\left\{ \begin{array}{rcll} -\epsilon\Delta p + \mathbf{a}\cdot\nabla p & = & f & \text{in } \Omega, \\ p & = & g_D & \text{on } \Gamma_D, \\ \mathbf{n}\cdot\nabla p & = & g_N & \text{on } \Gamma_N, \end{array} \right. \tag{1}$$

where: $\Delta \equiv \frac{\partial^2}{\partial x^2} + \frac{\partial^2}{\partial y^2}$ is the Laplacian; $\nabla \equiv (\frac{\partial}{\partial x}, \frac{\partial}{\partial y})^t$ is the gradient operator; $\mathbf{a} = (a(x,y), b(x,y))^t$, $f = f(x,y)$, $g_D = g_D(x,y)$, and $g_N = g_N(x,y)$ are given functions; $\epsilon > 0$ is a given constant (which determines the size of diffusion relative to convection); and $\mathbf{n}$ is the outward unit normal vector on the boundary $\partial\Omega$. For focus, we restrict our attention to two dimensions and Laplacian second-order terms, but the approach we develop can be extended to higher dimensions and variable coefficients cases. The basic FOSLS approach also provides a simplified setting for treating nonlinearity (cf. [2]), although the scaling we introduce below would no doubt require special consideration. Under general assumptions on (1), we can use standard variational arguments (e.g., the Lax–Milgram theorem; cf. [8]) to establish existence and uniqueness of the solution p in $H^1(\Omega)$.

2.2. FOSLS methodology. The usual FOSLS methodology for solving problem (1) numerically is described in [5, 6]. The starting point of this approach is to introduce a new vector variable $\mathbf{u} = (u, v)^t$, defined as the gradient of p. With this defining equation and a corresponding curl-free condition, together with the Dirichlet boundary conditions on p and inherited boundary conditions on $\mathbf{u}$, we can then reformulate problem (1) as the following first-order system:

$$\left\{\begin{array}{rcll} \mathbf{u} - \nabla p &=& 0 & \text{in } \Omega, \\ -\nabla\cdot\mathbf{u} + \frac{1}{\epsilon}\mathbf{a}\cdot\nabla p &=& \frac{1}{\epsilon}f & \text{in } \Omega, \\ \nabla\times\mathbf{u} &=& 0 & \text{in } \Omega, \\ p &=& g_D & \text{on } \Gamma_D, \\ \mathbf{n}\cdot\mathbf{u} &=& g_N & \text{on } \Gamma_N, \\ \mathbf{n}\times\mathbf{u} &=& \frac{\partial g_D}{\partial\tau} & \text{on } \Gamma_D, \end{array}\right. \tag{2}$$

where $\nabla\cdot \equiv (\frac{\partial}{\partial x}, \frac{\partial}{\partial y})$ is the divergence operator; $\nabla\times \equiv (\frac{\partial}{\partial y}, -\frac{\partial}{\partial x})$ is the curl operator; and $\frac{\partial}{\partial\tau}$ is the derivative on $\partial\Omega$ in the tangential counter-clockwise direction. We defer specific assumptions on the coefficients, data, and domain to the theoretical discussion of the next subsection because our focus here is on the methodology.

In addition to the usual Sobolev space definitions and notation [9, 16], we need to introduce special spaces for $\mathbf{u}$ and p. Letting n be a positive integer, $(\cdot,\cdot)_0$ the inner product and $\|\cdot\|_0$ the induced norm on $L^2(\Omega)^n$, and $\mathbf{g} = (g_D, g_N)$, then define the linear varieties

$$\mathbf{W}^{\mathbf{g}}(\mathrm{div};\Omega) = \{\mathbf{v}\in H(\mathrm{div};\Omega) : \mathbf{n}\cdot\mathbf{v} = g_N \text{ on } \Gamma_N\},$$

$$\mathbf{W}^{\mathbf{g}}(\mathrm{curl};\Omega) = \left\{\mathbf{v}\in H(\mathrm{curl};\Omega) : \mathbf{n}\times\mathbf{v} = \frac{\partial g_D}{\partial\tau} \text{ on } \Gamma_D\right\},$$

$$\mathbf{W}^{\mathbf{g}} = \mathbf{W}^{\mathbf{g}}(\mathrm{div};\Omega)\cap\mathbf{W}^{\mathbf{g}}(\mathrm{curl};\Omega),$$

and

$$V^{\mathbf{g}} = \left\{q\in H^1(\Omega) : q = g_D \text{ on } \Gamma_D \text{ if } \Gamma_D\neq\emptyset, \int_\Omega q(\mathbf{x})d\mathbf{x} = 0 \text{ if } \Gamma_D = \emptyset\right\}.$$

Define the quadratic functional associated with problem (2) by

$$\begin{aligned} G_\epsilon(\mathbf{v},q;f,\mathbf{g}) &= \|\mathbf{v}-\nabla q\|_0^2 + \|-\nabla\cdot\mathbf{v} + \frac{1}{\epsilon}\mathbf{a}\cdot\nabla q - \frac{1}{\epsilon}f\|_0^2 + \|\nabla\times\mathbf{v}\|_0^2 \\ &\qquad \forall(\mathbf{v},q)\in\mathbf{W}^{\mathbf{g}}\times V^{\mathbf{g}}. \end{aligned} \tag{3}$$

The least-squares problem for (1) is then to minimize $G_\epsilon(\mathbf{v},q;f,\mathbf{g})$ over $\mathbf{W}^{\mathbf{g}}\times V^{\mathbf{g}}$: find $(\mathbf{u},p)\in\mathbf{W}^{\mathbf{g}}\times V^{\mathbf{g}}$ such that

$$G_\epsilon(\mathbf{u},p;f,\mathbf{g}) = \inf_{(\mathbf{v},q)\in\mathbf{W}^{\mathbf{g}}\times V^{\mathbf{g}}} G_\epsilon(\mathbf{v},q;f,\mathbf{g}). \tag{4}$$

Define the bilinear form $\mathcal{F}_\epsilon(\cdot;\cdot) : (\mathbf{W}^{\mathbf{g}}\times V^{\mathbf{g}})\times(\mathbf{W}^{\mathbf{0}}\times V^0)\to\mathbf{R}$ by

$$\begin{aligned} \mathcal{F}_\epsilon(\mathbf{u},p;\mathbf{v},q) &= (\mathbf{u}-\nabla p, \mathbf{v}-\nabla q)_0 \\ &\quad + \left(-\nabla\cdot\mathbf{u} + \frac{1}{\epsilon}\mathbf{a}\cdot\nabla p, -\nabla\cdot\mathbf{v} + \frac{1}{\epsilon}\mathbf{a}\cdot\nabla q\right)_0 \\ &\quad + (\nabla\times\mathbf{u}, \nabla\times\mathbf{v})_0 \end{aligned} \tag{5}$$

and the linear form $\mathcal{L}_\epsilon(\cdot,\cdot) : \mathbf{W^0} \times V^0 \to \mathbf{R}$ by

$$\mathcal{L}_\epsilon(\mathbf{v}, q) = \left(\frac{1}{\epsilon} f, -\nabla\cdot\mathbf{v} + \frac{1}{\epsilon}\mathbf{a}\cdot\nabla q\right)_0 . \tag{6}$$

Then the variational problem associated with (4) is to find $(\mathbf{u}, p) \in \mathbf{W^g} \times V^{\mathbf{g}}$ such that

$$\mathcal{F}_\epsilon(\mathbf{u}, p; \mathbf{v}, q) = \mathcal{L}_\epsilon(\mathbf{v}, q) \qquad \forall (\mathbf{v}, q) \in \mathbf{W^0} \times V^0. \tag{7}$$

In what follows, we will assume that $\mathbf{g} = (g_D, g_N) = \mathbf{0}$ unless otherwise stated. This assumption is without loss of generality because theory for the case $\mathbf{g} \neq \mathbf{0}$ can be handled in the usual way by determining a suitable q that satisfies the boundary conditions in (1), then rewriting the equation (1) in terms of correction $\tilde{p} = p - q$. In any event, when $\mathbf{g} = \mathbf{0}$, the superscript $\mathbf{g}$ will be dropped from the space notation (e.g., $\mathbf{W}$ denotes $\mathbf{W^0}$). Assuming that $f \in L^2(\Omega)$ ($f \in L^2(\Omega)/\mathbf{R}$ when $\Gamma_D = \emptyset$) and imposing general conditions that imply unique solvability of (1) (cf. [6]), we are assured of existence of the unique minimum $G_\epsilon(\mathbf{u}, p; f, \mathbf{0})$ over $\mathbf{W} \times V$, and that it corresponds to the solution of (1) in the sense that p solves (1) and $\mathbf{u} = \nabla p$.

REMARK 1. *We can write $\mathcal{F}_\epsilon(\mathbf{u}, p; \mathbf{v}, q) = (L(\mathbf{u}, p), L(\mathbf{v}, q))_0$, where the first-order operator L_ϵ is defined in block form by*

$$L_\epsilon = \begin{pmatrix} I & -\nabla \\ -\nabla\cdot & \frac{1}{\epsilon}\mathbf{a}\cdot\nabla \\ \nabla\times & 0 \end{pmatrix}. \tag{8}$$

REMARK 2. *Our definition of V ensures the Poincaré–Friedrichs inequality*

$$\|p\|_0 \leq C\|\nabla p\|_0^2$$

for some constant $C > 0$, depending only on Ω, and for all $p \in V$.

2.3. Well posedness. The principal theoretical result [6] that governs our FOSLS formulation is the equivalence on $\mathbf{W}\times V$ of the functional $G_\epsilon(\mathbf{u}, p; 0, \mathbf{0})$ and the squared H^1 norm of $(\mathbf{u}, p)$. In other words, $G_\epsilon(\mathbf{u}, p; 0, \mathbf{0})$ is bounded and coercive (elliptic) in the $H^1(\Omega)^3$ norm. For this result, we need several assumptions.

ASSUMPTION 1. *When $\Gamma_D \neq \emptyset$, for any $f \in H^{-1}(\Omega)$, the weak form associated with (1) is invertible in $H^1(\Omega)$. When $\Gamma_D = \emptyset$, for any $f \in H^{-1}(\Omega)/\mathbf{R}$, the weak form associated with (1) is invertible in $H^1(\Omega)/\mathbf{R}$.*

ASSUMPTION 2. *The domain Ω is bounded, open, and connected in $\mathbf{R}^2$, with boundary $\partial\Omega$ that consists of a finite number of disjoint, simple, closed curves Γ_i, $i = 0, \ldots, L$; Γ_0 is the piecewise $C^{1,1}$ outer boundary and Γ_i, $i = 1, \ldots, L$, are $C^{1,1}$ boundaries of a finite number of disjoint holes in Ω.*

ASSUMPTION 3. *The boundary is divided into Dirichlet and Neumann parts: $\partial\Omega = \Gamma_D \cup \Gamma_N$ such that $\Gamma_i \subseteq \Gamma_D$ for $i \in D$ and $\Gamma_i \subseteq \Gamma_N$ for $i \in N$ with $D \cup N = \{1, \ldots, L\}$. Γ_0 is divided into a finite number of connected pieces: $\Gamma_0 = \cup_{i=1,\ldots,M}\Gamma_{0,i}$ such that $\Gamma_{0,i} \subseteq \Gamma_D$ for $i \in D_0$ and $\Gamma_{0,i} \subseteq N_0$ for $i \in N_0$; since Γ_0 is a simple closed curve, M is even.*

ASSUMPTION 4. *Any point $\mathbf{x} \in \partial\Omega$ that separates Γ_D, and Γ_N must be a corner of $\partial\Omega$ with interior angle no larger than $\frac{\pi}{2}$.*

Assumptions 1–4 assure that, for any $f \in L^2(\Omega)$ ($L^2(\Omega)/\mathbf{R}$ when $\Gamma_D = \emptyset$), the solution of boundary value problem (1) is in $H^2(\Omega)$. These assumptions also imply

equivalence of $G_\epsilon(\mathbf{u}, p; 0, \mathbf{0})$ and the square of the $H^1(\Omega)^3$ norm $\|\cdot\|_1$ on $\mathbf{W} \times V$, as the following theorem (cf. [6]) asserts. Here we use subscripts to show the likely dependence of the equivalence constants on ϵ.

THEOREM 1. *Under assumptions* 1–4, *there exist positive constants* λ_ϵ *and* μ_ϵ, *depending only on* Ω *and* ϵ, *such that*

$$\lambda_\epsilon \left(\|\mathbf{u}\|_1^2 + \|p\|_1^2 \right) \leq G_\epsilon(\mathbf{u}, p; 0, \mathbf{0}) \leq \mu_\epsilon \left(\|\mathbf{u}\|_1^2 + \|p\|_1^2 \right) \tag{9}$$

for all $\mathbf{u} = (u, v)^t \in \mathbf{W}$ *and* $p \in V$.

2.4. Finite element approximation properties. Let T_h be a regular triangulation of Ω with elements of size $\mathcal{O}(h)$ on which we have defined two finite element approximation subspaces

$$\mathbf{W}_h \subset \mathbf{W} \text{ and } V_h \subset V$$

satisfying the inverse assumption (see [8]). The Rayleigh–Ritz finite element approximation to (7) is to find $(\mathbf{u}_h, p_h) \in \mathbf{W}_h \times V_h$ such that

$$\mathcal{F}_\epsilon(\mathbf{u}_h, p_h; \mathbf{v}, q) = \mathcal{L}_\epsilon(\mathbf{v}, q) \qquad \forall (\mathbf{v}, q) \in \mathbf{W}_h \times V_h. \tag{10}$$

For simplicity, we consider only the continuous piecewise linear finite element spaces

$$\mathbf{W}_h = \{\mathbf{v} = (w, z) \in C^0(\Omega)^2 \cap \mathbf{W} \,:\, w, z|_K \in P^1(K) \,\forall K \in T_h\},$$

$$V_h = \{q \in C^0(\Omega) \cap V \,:\, q|_K \in P^1(K) \,\forall K \in T_h\},$$

where $P^1(K)$ is the space of polynomials of degree at most one. The following theorem is established in [6].

THEOREM 2. *Assume that the solution,* $(\mathbf{u}, p)$, *of* (7) *is in* $H^{1+\eta}(\Omega)^3$ *for some* $\eta \in [0, 1]$, *and let* $(\mathbf{u}_h, p_h) \in \mathbf{W}_h \times V_h$ *be the solution of* (10). *Then*

$$\|p - p_h\|_1 + \|\mathbf{u} - \mathbf{u}_h\|_1 \leq C_\epsilon h^\eta \left(\|p\|_{1+\eta} + \|\mathbf{u}\|_{1+\eta} \right), \tag{11}$$

where the constant C_ϵ *depends only on* Ω *and* ϵ.

The results of Theorems 1 and 2 are strong in the sense that they establish coercivity and boundedness of G_ϵ, and the attendant approximation properties of standard finite elements, in the $H^1(\Omega)^3$ norm. Moreover, the equivalence asserted in (9) immediately implies optimal convergence of standard multigrid solvers (cf. [6]). Unfortunately, the relevant constants λ_ϵ, μ_ϵ, and C_ϵ almost certainly depend critically on ϵ. For small $\epsilon > 0$, these constants, and the performance of the discretization and solver schemes, will likely degrade.

3. Exponentially weighted least squares.

3.1. Motivation. A FOSLS approach based on the functional defined in (3) would likely not be able to achieve optimal performance uniformly in ϵ. The overall performance assessment must take into account not only the discretization error but also the convergence properties of whatever multigrid algorithm we choose (preferably one that is as simple and unspecialized as possible). We show here by formal reasoning that standard multigrid methods applied to the functional in (3) cannot achieve the performance we seek for small ϵ. (It should be clear from this reasoning that standard finite element methods would also have trouble in this regime.) Now, restricting our

attention for simplicity to, say, $C_0^\infty(\Omega)$ functions, then we can rewrite the bilinear form $\mathcal{F}_\epsilon$ as

$$\mathcal{F}_\epsilon(\mathbf{u},p;\mathbf{v},q) = (L_\epsilon^* L_\epsilon(\mathbf{u},p),(\mathbf{v},q))_0,$$

where L_ϵ^* is the formal adjoint of L_ϵ defined in (8). The "formal normal" least-squares operator $L_\epsilon^* L_\epsilon$ is given by

$$\begin{aligned} L_\epsilon^* L_\epsilon &= \begin{pmatrix} I & \nabla & T\nabla \\ \nabla\cdot & (\frac{1}{\epsilon}\mathbf{a}\cdot\nabla)^* & 0 \end{pmatrix} \begin{pmatrix} I & -\nabla \\ -\nabla\cdot & \frac{1}{\epsilon}\mathbf{a}\cdot\nabla \\ \nabla\times & 0 \end{pmatrix} \\ &= \begin{pmatrix} I-\Delta & -\nabla(I-\frac{1}{\epsilon}\mathbf{a}\cdot\nabla) \\ (I-(\frac{1}{\epsilon}\mathbf{a}\cdot\nabla)^*)\nabla\cdot & -\Delta+(\frac{1}{\epsilon}\mathbf{a}\cdot\nabla)^*(\frac{1}{\epsilon}\mathbf{a}\cdot\nabla) \end{pmatrix}, \end{aligned} \tag{12}$$

where $T = \left(\begin{smallmatrix} 0 & -1 \\ 1 & 0 \end{smallmatrix}\right)$. To see where the trouble comes for small ϵ, it is enlightening to simplify this formal normal as much as possible by restricting attention to constant coefficients and one dimension. Thus, $\mathbf{a} = \pm 1$ and the rescaling $p \to \pm\frac{1}{\epsilon}p$ yields

$$L_\epsilon^* L_\epsilon = \begin{pmatrix} I-\frac{\partial^2}{\partial x^2} & \frac{\partial^2}{\partial x^2} \\ \frac{\partial^2}{\partial x^2} & -\frac{\partial^2}{\partial x^2} \end{pmatrix} + \mathcal{O}(\epsilon). \tag{13}$$

The trouble is now apparent because error components of the form $(p,p)^t$ (i.e., $u = p$) that are oscillatory (i.e., $\|p\|_1 >> \|p\|_0$) yield relatively small residuals (i.e., $\|L_\epsilon^* L_\epsilon(p,p)^t\|_0 \approx \|p\|_0 + \mathcal{O}(\epsilon)\|p\|_1$). Clearly, this signals degradation of $H^1(\Omega)^3$ ellipticity. Now, if we ignore for the moment the issues of smoothness and boundary conditions, then associated least-squares problem (4) can be viewed as that of minimizing the error with respect to the norm

$$(L_\epsilon^* L_\epsilon(\mathbf{u},p),(\mathbf{u},p))_0^{\frac{1}{2}}.$$

As (13) shows, this norm exhibits increased coupling between $\mathbf{u}$ and p as ϵ becomes small. This means that standard multigrid algorithms will degrade when the convective part begins to dominate the diffusive part because the matrix of the associated linear system, which is just the discretization of $L_\epsilon^* L_\epsilon$, will begin to lose diagonal dominance. The multigrid solver must then take $\mathbf{u}$-p coupling into account, and this can be quite tricky to do in general. The situation is aggravated in two dimensions because the scales in the streamwise and cross-stream directions tend to exhibit completely different elliptic character as ϵ tends to zero.

REMARK 3. *If we replace* $\frac{1}{\epsilon}\mathbf{a}\cdot\nabla$ *by* $\frac{1}{\epsilon}\mathbf{a}\cdot\mathbf{u}$ *in the second equation in* (2)*, then we relieve the troublesome coupling between* $\mathbf{u}$ *and* p*. Unfortunately, this comes at the cost of increasing the coupling between the components* u *and* v*. To see the effects of this reformulation of* (2)*, note that the associated first-order least-squares operator becomes*

$$L_\epsilon = \begin{pmatrix} I & -\nabla \\ -\nabla\cdot+\frac{1}{\epsilon}\mathbf{a}\cdot & 0 \\ \nabla\times & 0 \end{pmatrix}.$$

The formal normal least-squares operator is therefore

$$\begin{aligned} L_\epsilon^* L_\epsilon &= \begin{pmatrix} I & \nabla+\frac{1}{\epsilon}\mathbf{a} & T\nabla \\ \nabla\cdot & 0 & 0 \end{pmatrix} \begin{pmatrix} I & -\nabla \\ -\nabla\cdot+\frac{1}{\epsilon}\mathbf{a}\cdot & 0 \\ \nabla\times & 0 \end{pmatrix} \\ &= \begin{pmatrix} I-\Delta+\frac{1}{\epsilon}\mathbf{a}(-\nabla\cdot+\frac{1}{\epsilon}\mathbf{a}\cdot)+\nabla\frac{1}{\epsilon}\mathbf{a}\cdot & -\nabla \\ \nabla\cdot & -\Delta \end{pmatrix}. \end{aligned}$$

Note that the coupling between $\mathbf{u}$ *and* p *in* $L_\epsilon^* L_\epsilon$ *is expressed by the off-diagonal terms, which are the first-order differential operators* $\nabla\cdot$ *and* $-\nabla$*. These terms are dominated by the second-order diagonal terms for any scale* $\epsilon > 0$*. This suggests that the multigrid solver can be designed essentially as if* $\mathbf{u}$ *and* p *are decoupled. For example, we could expect good performance from a block Gauss–Seidel process that uses fast solvers for* $\mathbf{u}$ *and* p *individually. However, the problem here would be to develop a fast solver for* $\mathbf{u}$*: even though* $\mathbf{u}$ *could be treated almost independently of* p*, the components of* $\mathbf{u}$ *would be strongly coupled for small* ϵ*, and this would demand a much more complicated multigrid solver.*

3.2. Exponentially weighted least squares. Our objective, then, is to reformulate our FOSLS approach to problem (1) so that the new functional G_ϵ yields a formal normal that, uniformly in ϵ, is diagonally dominant—not just in the block $\mathbf{u}$-p sense but in the full u-v-p sense. In other words, our aim is to redefine G_ϵ so that an equivalent relation analogous to (9) holds but with constants λ_ϵ and μ_ϵ that do not depend on ϵ. We will see that an exponential weighting of G_ϵ, and an analogous weighting of the $H^1(\Omega)^3$ norm in (9), accomplishes this in some generality.

To motivate the scaling that we choose, consider the exponential transformation of the convection-diffusion equation in (1) that yields

$$-e^{\alpha}(e^{-\alpha}p_x)_x - e^{\beta}(e^{-\beta}p_y)_y = \frac{1}{\epsilon}f,$$

where $\alpha = \alpha(x,y)$ and $\beta = \beta(x,y)$ are chosen so that $\alpha_x = \frac{a}{\epsilon}$ and $\beta_y = \frac{b}{\epsilon}$. This leads us naturally to the exponentially scaled form of (2) given by

$$\left\{\begin{array}{rcll} e^{\alpha}u - p_x &=& 0 & \text{in } \Omega,\\ e^{\beta}v - p_y &=& 0 & \text{in } \Omega,\\ -e^{\alpha}u_x - e^{\beta}v_y &=& \frac{1}{\epsilon}f & \text{in } \Omega,\\ (e^{\alpha}u)_y - (e^{\beta}v)_x &=& 0 & \text{in } \Omega,\\ p &=& g_D & \text{on } \Gamma_D,\\ \mathbf{n}\cdot e^{\boldsymbol{\alpha}}\mathbf{u} &=& g_N & \text{on } \Gamma_N,\\ \mathbf{n}\times e^{\boldsymbol{\alpha}}\mathbf{u} &=& \frac{\partial g_D}{\partial \tau} & \text{on } \Gamma_D, \end{array}\right. \tag{14}$$

where $e^{\boldsymbol{\alpha}}\mathbf{u} = (e^{\alpha}u, e^{\beta}v)^t$. Unfortunately, when we take the sum of L^2 norms of the equations in (14), the third and fourth equations produce cross terms:

$$2(e^{\alpha}u_x, e^{\beta}v_y)_0 - 2((e^{\alpha}u)_y, (e^{\beta}v)_x)_0,$$

which generally induce strong coupling between u and v in the associated bilinear form. To weaken this coupling, we use a rescaling of these two equations (and a commensurate rescaling of the first two equations in (14)) to obtain

$$\left\{\begin{array}{rcll} e^{\frac{\alpha-\beta}{2}}u - e^{-\frac{\alpha+\beta}{2}}p_x &=& 0 & \text{in } \Omega,\\ e^{\frac{\beta-\alpha}{2}}v - e^{-\frac{\alpha+\beta}{2}}p_y &=& 0 & \text{in } \Omega,\\ -e^{\frac{\alpha-\beta}{2}}u_x - e^{\frac{\beta-\alpha}{2}}v_y &=& e^{-\frac{\alpha+\beta}{2}}\frac{1}{\epsilon}f & \text{in } \Omega,\\ e^{-\frac{\alpha+\beta}{2}}(e^{\alpha}u)_y - e^{-\frac{\alpha+\beta}{2}}(e^{\beta}v)_x &=& 0 & \text{in } \Omega,\\ p &=& g_D & \text{on } \Gamma_D,\\ \mathbf{n}\cdot e^{\boldsymbol{\alpha}}\mathbf{u} &=& g_N & \text{on } \Gamma_N,\\ \mathbf{n}\times e^{\boldsymbol{\alpha}}\mathbf{u} &=& \frac{\partial g_D}{\partial \tau} & \text{on } \Gamma_D. \end{array}\right. \tag{15}$$

Our exponentially scaled functional for $\mathbf{v} = (w, z)$ then becomes

$$\begin{aligned} G_\epsilon(\mathbf{v}, q; f, \mathbf{g}) &= \|e^{\frac{\alpha-\beta}{2}} w - e^{-\frac{\alpha+\beta}{2}} q_x\|_0^2 + \|e^{\frac{\beta-\alpha}{2}} z - e^{-\frac{\alpha+\beta}{2}} q_y\|_0^2 \\ &\quad + \|e^{\frac{\alpha-\beta}{2}} w_x + e^{\frac{\beta-\alpha}{2}} z_y + e^{-\frac{\alpha+\beta}{2}} \frac{1}{\epsilon} f\|_0^2 \\ &\quad + \|e^{-\frac{\alpha+\beta}{2}} (e^{\alpha} w)_y - e^{-\frac{\alpha+\beta}{2}} (e^{\beta} z)_x\|_0^2. \end{aligned} \tag{16}$$

Again, without loss of generality, we assume that $\mathbf{g} = \mathbf{0}$, so that the minimization problem for (16) is to find $(\mathbf{u}, p) \in \mathbf{W} \times V$ such that

$$G_\epsilon(\mathbf{u}, p; f, \mathbf{0}) = \inf_{(\mathbf{v}, q) \in \mathbf{W} \times V} G_\epsilon(\mathbf{v}, q; f, \mathbf{0}). \tag{17}$$

Define the bilinear form $\mathcal{F}_\epsilon(\cdot;\cdot) : (\mathbf{W} \times V)^2 \to \mathbf{R}$ by

$$\begin{aligned} \mathcal{F}_\epsilon(\mathbf{u}, p; \mathbf{v}, q) &= (e^{\frac{\alpha-\beta}{2}} u - e^{-\frac{\alpha+\beta}{2}} p_x, e^{\frac{\alpha-\beta}{2}} w - e^{-\frac{\alpha+\beta}{2}} q_x)_0 \\ &\quad + (e^{\frac{\beta-\alpha}{2}} v - e^{-\frac{\alpha+\beta}{2}} p_y, e^{\frac{\beta-\alpha}{2}} z - e^{-\frac{\alpha+\beta}{2}} q_y)_0 \\ &\quad + (e^{\frac{\alpha-\beta}{2}} u_x + e^{\frac{\beta-\alpha}{2}} v_y, e^{\frac{\alpha-\beta}{2}} w_x + e^{\frac{\beta-\alpha}{2}} z_y)_0 \\ &\quad + (e^{-\frac{\alpha+\beta}{2}} (e^{\alpha} u)_y - e^{-\frac{\alpha+\beta}{2}} (e^{\beta} u)_x, \\ &\qquad\qquad e^{-\frac{\alpha+\beta}{2}} (e^{\alpha} w)_y - e^{-\frac{\alpha+\beta}{2}} (e^{\beta} z)_x)_0 \end{aligned} \tag{18}$$

and the linear form $\mathcal{L}_\epsilon(\cdot,\cdot) : \mathbf{W} \times V \to \mathbf{R}$ by

$$\mathcal{L}_\epsilon(\mathbf{v}, q) = \left(e^{-\frac{\alpha+\beta}{2}} \frac{1}{\epsilon} f, e^{\frac{\alpha-\beta}{2}} w_x + e^{\frac{\beta-\alpha}{2}} z_y \right)_0. \tag{19}$$

Then the variational problem associated with (17) is to find $(\mathbf{u}, p) \in \mathbf{W} \times V$ such that

$$\mathcal{F}_\epsilon(\mathbf{u}, p; \mathbf{v}, q) = \mathcal{L}_\epsilon(\mathbf{v}, q) \qquad \forall (\mathbf{v}, q) \in \mathbf{W} \times V. \tag{20}$$

As before, when $f \in L^2(\Omega)$ ($f \in L^2(\Omega)/\mathbf{R}$ when $\Gamma_D = \emptyset$) and under general conditions that imply that problem (1) is uniquely solvable, we are guaranteed of existence of the unique minimum of $G_\epsilon(\mathbf{u}, q; f)$ over $\mathbf{W} \times V$ and that it corresponds to the solution of (1) in the sense that p solves (1) and $u = e^{-\alpha} p_x$ and $v = e^{-\beta} p_y$.

Remark 4. *Assume for discussion that we have the separable case where α and β can be chosen so that, in addition to $\alpha_x = \frac{a}{\epsilon}$ and $\beta_y = \frac{b}{\epsilon}$, we have $\alpha_y = \beta_x = 0$ (in which case we must have $a_y = b_x = 0$). We can then write $\mathcal{F}_\epsilon(\mathbf{u}, p; \mathbf{v}, q) = (L_\epsilon(u, v, p), L_\epsilon(w, z, q))_0$, where L_ϵ is defined by*

$$L_\epsilon = \begin{pmatrix} e^{\frac{\alpha-\beta}{2}} & 0 & -e^{-\frac{\alpha+\beta}{2}} \frac{\partial}{\partial x} \\ 0 & e^{\frac{\beta-\alpha}{2}} & -e^{-\frac{\alpha+\beta}{2}} \frac{\partial}{\partial y} \\ e^{\frac{\alpha-\beta}{2}} \frac{\partial}{\partial x} & e^{\frac{\beta-\alpha}{2}} \frac{\partial}{\partial y} & 0 \\ e^{\frac{\alpha-\beta}{2}} \frac{\partial}{\partial y} & -e^{\frac{\beta-\alpha}{2}} \frac{\partial}{\partial x} & 0 \end{pmatrix}. \tag{21}$$

The formal normal least-squares operator $L_\epsilon^* L_\epsilon$ is then given by

$$L_\epsilon^* L_\epsilon = \begin{pmatrix} e^{\alpha-\beta} I - \nabla \cdot e^{\alpha-\beta} \nabla & 0 & -e^{-\beta} \frac{\partial}{\partial x} \\ 0 & e^{\beta-\alpha} I - \nabla \cdot e^{\beta-\alpha} \nabla & -e^{-\alpha} \frac{\partial}{\partial y} \\ \frac{\partial}{\partial x} e^{-\beta} & \frac{\partial}{\partial y} e^{-\alpha} & -\nabla \cdot e^{-\alpha-\beta} \nabla \end{pmatrix}. \tag{22}$$

It is easy to see that the principal part of $L_\epsilon^* L_\epsilon$ is diagonally dominant uniformly in ϵ: let $\mathcal{D}$ denote the block diagonal part of $L_\epsilon^* L_\epsilon$; then the principal part of the off-diagonal entries of $\mathcal{D}^{-\frac{1}{2}} L_\epsilon^* L_\epsilon \mathcal{D}^{-\frac{1}{2}}$ are generally bounded in norm by some constant $\delta < 1$ uniformly in ϵ. This formal diagonal dominance property suggests that $G_\epsilon(\mathbf{u}, p; 0, \mathbf{0})$ is uniformly equivalent to the square of the exponentially scaled $H^1(\Omega)^3$ norm $\|\cdot\|_e$ defined by

$$\begin{aligned} \|(\mathbf{u}, p)\|_e = (&\|e^{\frac{\alpha-\beta}{2}} \nabla u\|_0^2 + \|e^{\frac{\beta-\alpha}{2}} \nabla v\|_0^2 \\ &+ \|e^{\frac{\alpha-\beta}{2}} u\|_0^2 + \|e^{\frac{\beta-\alpha}{2}} v\|_0^2 \\ &+ \|e^{-\frac{\alpha+\beta}{2}} \nabla p\|_0^2)^{\frac{1}{2}}. \end{aligned} \tag{23}$$

We will also use analogous notation for the scaled $H^1(\Omega)^2$ seminorm

$$|\mathbf{u}|_e = \left(\|e^{\frac{\alpha-\beta}{2}} \nabla u\|_0^2 + \|e^{\frac{\beta-\alpha}{2}} \nabla v\|_0^2 \right)^{\frac{1}{2}}. \tag{24}$$

The exponentially scaled functionals and norms we use here come directly from our attempt to achieve numerical performance that is uniform in ϵ. The point here is that the usual (unscaled) H^1 norm is too strong a measure by which to observe uniformity. Other approaches (cf. [10, 12]) weaken the H^1 norm by scaling the H^1 seminorm by ϵ:

$$\|p\|_\epsilon := \left(\epsilon \|\nabla p\|_0^2 + \|p\|_0^2 \right)^{1/2}.$$

This global scaling weakens the H^1 norm over the whole domain. The advantage of our pointwise exponential scaling is that this weakening occurs only in those regions of the domain (e.g., boundary layers) where it is needed.

There are several inherent benefits that come with this uniform equivalence, which stem from the fact that it amounts to decomposing the problem into three loosely coupled scalar equations, each of which are elliptic and bounded in their individual scaled H^1 norms as expressed in (23). This means that design of discretization and algebraic solution can be individualized to each of these scalar equations, thus allowing for standard finite elements and the most basic multigrid schemes. Of course, the most effective discretization must take the evolving solution into account by allowing the possible use of special elements and/or nonuniform grids. This possibility makes this equivalence all the more important because it allows the adaptive process to concentrate on the individual variables, with little concern for their interaction.

REMARK 5. *Another feature of FOSLS is that the functional $G_\epsilon(\mathbf{u}, p; f, \mathbf{g})$ itself provides a sharp measure of the total accuracy (in the sense of $\|\cdot\|_e$). Suppose for discussion that $\mathbf{g} = \mathbf{0}$. Then $G_\epsilon^{\frac{1}{2}}(\mathbf{v}, q; f, \mathbf{0})$ is a measure of the absolute error in $(\mathbf{v}, q)$ as an approximation to the solution $(\mathbf{u}, p)$ of (15). Since*

$$G_\epsilon^{\frac{1}{2}}(\mathbf{0}, 0; f, \mathbf{0}) = G_\epsilon^{\frac{1}{2}}(\mathbf{u}, p; 0, \mathbf{0})$$

is a corresponding measure of the magnitude of $(\mathbf{u}, p)$, then the ratio

$$G_\epsilon^{\frac{1}{2}}(\mathbf{v}, q; f, \mathbf{0}) / G_\epsilon^{\frac{1}{2}}(\mathbf{0}, 0; f, \mathbf{0})$$

is a measure of the relative error in $(\mathbf{v}, q)$. This feature is important for adaptive refinement, as we will demonstrate in the next section.

One advantage of the special form of the $H^1(\Omega)^3$ equivalence that we have is that we can use a two-stage process to solve first for the flux $\mathbf{u}$, then for the original variable p (if necessary). To see this, consider the splitting

$$G_\epsilon(\mathbf{v},q;f,\mathbf{g}) = G_\epsilon^{(1)}\left(\mathbf{v};f,g_N,\frac{\partial g_D}{\partial\tau}\right) + G_\epsilon^{(2)}(q;\mathbf{v},g_D),$$

where writing $\mathbf{v}=(w,z)$ we define

$$\begin{aligned} G_\epsilon^{(1)}\left(\mathbf{v};f,g_N,\frac{\partial g_D}{\partial\tau}\right) &= \left\| e^{\frac{\alpha-\beta}{2}}w_x + e^{\frac{\beta-\alpha}{2}}z_y + e^{-\frac{\alpha+\beta}{2}}\frac{1}{\epsilon}f\right\|_0^2 \\ &\quad + \|e^{-\frac{\alpha+\beta}{2}}(e^\alpha w)_y - e^{-\frac{\alpha+\beta}{2}}(e^\beta z)_x\|_0^2, \end{aligned} \tag{25}$$

$$G_\epsilon^{(2)}(q;\mathbf{v},g_D) = \|e^{-\frac{\alpha+\beta}{2}}q_x - e^{\frac{\alpha-\beta}{2}}w\|_0^2 + \|e^{-\frac{\alpha+\beta}{2}}q_y - e^{\frac{\beta-\alpha}{2}}z\|_0^2. \tag{26}$$

Analogous to the two-stage scheme introduced in [7], we can approximate $\mathbf{u}$ in the first stage by minimizing $G_\epsilon^{(1)}(\mathbf{v};f,g_N,\frac{\partial g_D}{\partial\tau})$ alone over $\mathbf{v}\in\mathbf{W}^{\mathbf{g}}$. The variable p can then be recovered by minimizing $G_\epsilon^{(2)}(q;\mathbf{v},g_D)$ over $q\in V$, with $\mathbf{v}$ fixed as the approximation to $\mathbf{u}$ determined in the first stage. That the first stage can be accomplished efficiently and accurately, uniformly in ϵ, is confirmed for a model problem in the following theorem, which follows essentially by construction.

THEOREM 3. *Suppose that $a=a(x)$ and $b=b(y)$ are essentially bounded measurable functions on Ω so that $G_\epsilon^{(1)}(\mathbf{u};f,g_N,\frac{\partial g_D}{\partial\tau})$ is well defined on $\mathbf{W}^{\mathbf{g}}$ for appropriate $(f,g_N,\frac{\partial g_D}{\partial\tau})$. Consider the model domain of a rectangle whose sides are parallel to the coordinate axes. Then we have the precise equivalence relation*

$$G_\epsilon^{(1)}(\mathbf{u};0,0,0) = |\mathbf{u}|_e^2$$

for all $\mathbf{u}=(u,v)^t\in\mathbf{W}$.

Proof. We will prove this equivalence for $\mathbf{u}\in\mathbf{W}\cap C^\infty(\Omega)^2$; the general case $\mathbf{u}\in\mathbf{W}$ will then follow by continuity. But, for such $\mathbf{u}$, it is easy to see from $\mathbf{a}=(a(x),b(y))^t$ that

$$G_\epsilon^{(1)}(\mathbf{u};0,0,0) - |\mathbf{u}|_e^2 = (u_x,v_y)_0 - (u_y,v_x)_0 \tag{27}$$

$$= (\nabla u,\nabla^\perp v)_0, \tag{28}$$

where $\nabla^\perp v$ denotes the vector $(v_y,-v_x)^t$. By the divergence theorem, we then have

$$G_\epsilon^{(1)}(\mathbf{u};0,0,0) - |\mathbf{u}|_e^2 = -(u,\nabla\cdot\nabla^\perp v)_0 + \int_\Gamma u(\mathbf{n}\times\nabla^\perp v)\,ds.$$

The first term on the right-hand side vanishes because $\nabla\cdot\nabla^\perp = 0$. The second also vanishes by virtue of the boundary conditions imposed on $\mathbf{u}$: either $u=0$ or $v=0$ on Γ; but $v=0$ implies that $\mathbf{n}\times\nabla^\perp v = 0$ because it is the tangential derivative of v on Γ; in any case, $u(\mathbf{n}\times\nabla^\perp v)=0$. ∎

REMARK 6. *Theorem 3 is proved here only for the model case of a rectangle aligned with the coordinate axes. However, it should be clear that the proof extends to any domain that can be mapped smoothly to such a rectangle, provided we are able to define u and v so that they transform to respective functions of x and y alone. This*

suggests a possible strategy for formulating the least-squares functionals: define u to be the derivative of p in the streamwise direction and v to be the derivative of p in the cross-stream direction. The discretization would then require local *elementwise approximation to the streamwise direction $\frac{\mathbf{a}}{\|\mathbf{a}\|}$, but no problematic* global *coordinate transformation would be needed. Instead of exploring this approach here, we focus on the simpler coordinate definition of the components of $\mathbf{u} = \nabla p$.*

4. Numerical results. Here we focus on numerical results from discretization error studies of the exponentially weighted least squares functional. For the test cases studied here, we observed no difference between the functional and weighted $H^1(\Omega)^3$ error measures using (23) and (24). To measure discretization error, we therefore provide estimates of

$$\gamma_{\epsilon,N} = \left[\left(\inf_{(\mathbf{v}^N, q^N) \in \mathbf{W}^N \times V^N} G_\epsilon(\mathbf{v}^N, q^N; f, \mathbf{0}) \right) \Big/ G_\epsilon(\mathbf{0}, 0; f, \mathbf{0}) \right]^{\frac{1}{2}}$$

and

$$\gamma^{(1)}_{\epsilon,N} = \left[\left(\inf_{\mathbf{v}^N \in \mathbf{W}^N} G^{(1)}_\epsilon(\mathbf{v}^N; f, 0, 0) \right) \Big/ G^{(1)}_\epsilon(\mathbf{0}; f, 0, 0) \right]^{\frac{1}{2}},$$

where $\mathbf{W}^N$ and V^N denote our finite element subspaces of $\mathbf{W}$ and V, respectively, corresponding to grid N. Here, N signifies the number of elements in the given rectangular or composite rectangular grid $\mathcal{R}_N$ (in all our tests, we used the same grid for each of the variables, although in some cases noted below we use different types of elements). Our test are designed to measure the dependence of these estimates on N as well as ϵ. The ultimate goal is to achieve something analogous to $\mathcal{O}(h)$ or better asymptotic accuracy uniformly in ϵ. In fact, we hope to achieve estimates of the form

$$\gamma_{\epsilon,N} \leq C \left(\frac{1}{N} \right)^{\frac{\delta}{2}}, \tag{29}$$

where $\delta \geq 1$ and $C < \infty$ are independent of ϵ. For simplicity, the next subsection focuses on problems that can be treated by tensor-product grids and on tests of the first stage, $G^{(1)}_\epsilon$, involving only $\mathbf{u}$. The subsequent subsection allows for more general problems since composite grids with local refinements are used. The refinement strategy is based on using the functional itself as a local error measure. We demonstrate the effectiveness of a simple strategy based on this measure for G_ϵ as well as $G^{(1)}_\epsilon$. Finally, we end this section with some considerations on the multigrid solver, with results of convergence studies for the functional G_ϵ.

4.1. Tensor-product grids. Here we consider grids $\mathcal{R}_\mathcal{N}$ consisting for $1 \leq i, j \leq N^{\frac{1}{2}}$ of rectangles $R_{i,j}$ with corners $\{\mathrm{x}_{i-1,j-1}, \mathrm{x}_{i,j-1}, \mathrm{x}_{i,j}, \mathrm{x}_{i-1,j}\}$, where

$$\mathrm{x}_{i,j} = (x_i, y_j),\ 0 = x_0 < x_1 < \cdots < x_N = 1,\ 0 = y_0 < y_1 < \cdots < y_N = 1.$$

We concentrate on the values of $\gamma^{(1)}_{\epsilon,N}$ for fairly coarse grids, where the effects of convection are the strongest.

4.1.1. Example 1: Aligned flow and constant coefficients. Let $\Omega = [0,1] \times [0,1]$, $\Gamma_D = \partial\Omega$, $\Gamma_N = \emptyset$, $\mathbf{a} = (-1, 0)$, and $g_D = 0$, and define f so that $p(x, y) =$

TABLE 1
$\gamma^{(1)}_{\epsilon,N}\left(\frac{\gamma^{(1)}_{\epsilon,N}}{\gamma^{(1)}_{\epsilon,4N}}\right)$ *for tensor-product grids, Example* 1.

ϵ	$N = 4 \times 4$	$N = 8 \times 8$	$N = 16 \times 16$
1	$1.71\,10^{-1}$	$8.38\,10^{-2}$ (2.04)	$4.17\,10^{-2}$ (2.01)
$\frac{1}{2}$	$1.66\,10^{-1}$	$8.11\,10^{-2}$ (2.05)	$4.03\,10^{-2}$ (2.01)
$\frac{1}{4}$	$1.49\,10^{-1}$	$7.23\,10^{-2}$ (2.06)	$3.59\,10^{-2}$ (2.01)
$\frac{1}{8}$	$1.12\,10^{-1}$	$5.34\,10^{-2}$ (2.10)	$2.64\,10^{-2}$ (2.02)
$\frac{1}{16}$	$7.24\,10^{-2}$	$3.23\,10^{-2}$ (2.24)	$1.57\,10^{-2}$ (2.06)
$\frac{1}{32}$	$4.86\,10^{-2}$	$1.86\,10^{-2}$ (2.61)	$8.48\,10^{-3}$ (2.19)
$\frac{1}{64}$	$3.82\,10^{-2}$	$1.15\,10^{-2}$ (3.32)	$4.59\,10^{-3}$ (2.50)
$\frac{1}{128}$	$3.48\,10^{-2}$	$8.68\,10^{-3}$ (4.01)	$2.86\,10^{-3}$ (3.03)
$\frac{1}{256}$	$3.38\,10^{-2}$	$7.79\,10^{-3}$ (4.34)	$2.51\,10^{-3}$ (3.10)

$(x-x^2)(y-y^2)e^{-\frac{x}{\epsilon}}$ solves (1). Then $\mathbf{W} = \{\mathbf{u} \in H^1(\Omega)^2 : \mathbf{n} \times \mathbf{u} = 0 \text{ on } \partial\Omega\}$, and the exponentially weighted functional involving $\mathbf{u}$ only is

$$G^{(1)}_{\epsilon}(\mathbf{u}; f, \mathbf{0}) = \left\| e^{\frac{-x}{2\epsilon}} u_x + e^{\frac{x}{2\epsilon}} v_y + e^{\frac{x}{2\epsilon}} \frac{1}{\epsilon} f \right\|_0^2 + \| e^{\frac{-x}{2\epsilon}} u_y - e^{\frac{x}{2\epsilon}} v_x \|_0^2, \quad \mathbf{u} \in \mathbf{W}.$$

Its bilinear part is uniformly equivalent to the scaled $H^1(\Omega)^2$ seminorm

$$|\mathbf{u} - \mathbf{u}^N|_e = \left(\| e^{\frac{-x}{2\epsilon}} \nabla(u - u^N) \|_0^2 + \| e^{\frac{x}{2\epsilon}} \nabla(v - v^N) \|_0^2 \right)^{\frac{1}{2}}. \tag{30}$$

Note that the exact fluxes are

$$u = \left(1 - \left(\frac{1}{\epsilon} + 2\right) x + \frac{x^2}{\epsilon}\right)(y - y^2) \tag{31}$$

and

$$v = (x - x^2)(1 - 2y)e^{-\frac{x}{\epsilon}}, \tag{32}$$

so we may use continuous piecewise bilinear elements for u and continuous piecewise exponential-type elements for v. Our particular choice for basis elements for v amounts to rescaling the flux according to $v = \widehat{v} e^{\frac{-x}{\epsilon}}$, then using bilinear elements to approximate $\widehat{v}$. This effective rescaling of v means that the exact solution is smooth ($\widehat{v} = (x - x^2)(1 - 2y)$). Also, the solution is very smooth in the cross-stream direction, so we use uniform y-partitions. But, to accommodate possible boundary layers, we will approximately minimize the following functional in order to determine the x-partition:

$$\mathcal{G}(x_1, \ldots, x_{n-1}) = \sum_{i=0}^{N-1} \int_{x_i}^{x_{i+1}} e^{\frac{-x}{2\epsilon}} (x_{i+1} - x_i)^2 \, dx, \tag{33}$$

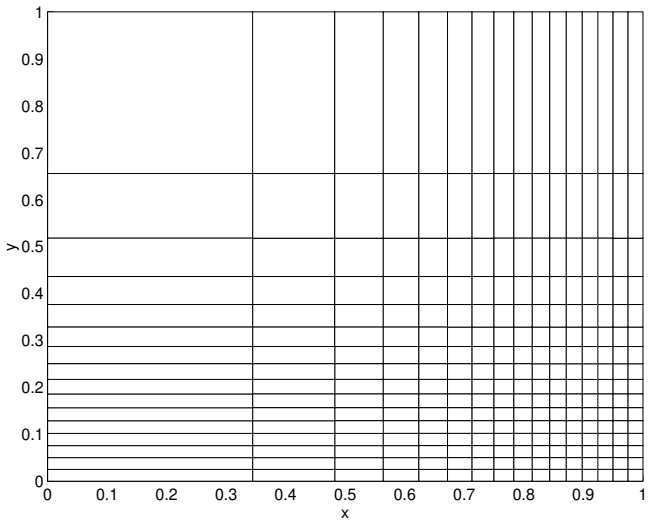

FIG. 1. *Grid in Example* 2 *for* $\epsilon = \frac{1}{32}$.

where $0 = x_0 < x_1 < \cdots < x_{n-1} < x_n = 1$. Table 1 depicts absolute (relative) estimates of errors computed by many multigrid cycles. These results suggest that the discretization error is $\mathcal{O}(\frac{1}{\sqrt{N}})$ (analogous to $\mathcal{O}(h)$ in the uniform grid case).

4.1.2. Example 2: Nonaligned flow and variable coefficients. Let $\Omega = [0,1] \times [0,1]$, $\Gamma_D = \partial\Omega$, $\Gamma_N = \emptyset$, $\mathbf{a} = (x, -y)$, and $g_D = xe^{\frac{x^2-1}{2\epsilon}} + (1-y)e^{-\frac{y^2}{2\epsilon}}$, and define f so that $p(x,y) = xe^{\frac{x^2-1}{2\epsilon}} + (1-y)e^{-\frac{y^2}{2\epsilon}}$ solves (1). Then the exponentially weighted functional involving $\mathbf{u}$ only is

$$G_\epsilon^{(1)}(\mathbf{u}; f, \mathbf{0}) = \|e^{\frac{x^2-1+y^2}{4\epsilon}} u_x + e^{\frac{-(x^2-1+y^2)}{4\epsilon}} v_y + e^{\frac{-(x^2-1-y^2)}{4\epsilon}} \frac{1}{\epsilon} f\|_0^2 + \|e^{\frac{x^2-1+y^2}{4\epsilon}} u_y - e^{\frac{-(x^2-1+y^2)}{4\epsilon}} v_x\|_0^2.$$

Using bilinear elements for *both* components of $\mathbf{u}$ ($u = 1 + \frac{x^2}{\epsilon}$, $v = -1 - \frac{y}{\epsilon} + \frac{y^2}{\epsilon}$), then considerations similar to that of Example 1 suggest that good approximation can be obtained by using x- and y-partitions obtained by minimizing the functionals

$$\mathcal{G}(x_1, \ldots, x_{n-1}) = \sum_{i=0}^{N-1} \int_{x_i}^{x_{i+1}} e^{\frac{x^2}{4\epsilon}} (x_{i+1} - x_i)^2 \, dx, \tag{34}$$

$$\mathcal{G}(y_1, \ldots, y_{n-1}) = \sum_{i=0}^{N-1} \int_{yi}^{y_{i+1}} e^{\frac{-y^2}{4\epsilon}} (y_{i+1} - y_i)^2 \, dy. \tag{35}$$

For $\epsilon = \frac{1}{32}$ and $N = 16 \times 16$, we obtained the grid depicted in Figure 1. Table 2 gives the results for this example, which show behavior similar to that for Example 1.

4.2. Composite grids. As a compromise between tensor-product and unstructured grids, here we use a composite grid scheme (cf. [15]). See Figure 2. The strategy we use for refinement is very simple: when the functional is below a prescribed tolerance, the process stops; until then, each element that contributes more than half

TABLE 2
$\gamma^{(1)}_{\epsilon,N}$ $\left(\frac{\gamma^{(1)}_{\epsilon,N}}{\gamma^{(1)}_{\epsilon,4N}}\right)$ *for tensor-product grids, Example* 2.

ϵ	$N = 4 \times 4$	$N = 8 \times 8$	$N = 16 \times 16$
1	$1.59\,10^{-1}$	$7.92\,10^{-2}$ (2.01)	$3.96\,10^{-2}$ (2.00)
$\frac{1}{2}$	$1.60\,10^{-1}$	$7.97\,10^{-2}$ (2.01)	$3.99\,10^{-2}$ (2.00)
$\frac{1}{4}$	$1.62\,10^{-1}$	$8.06\,10^{-2}$ (2.01)	$4.03\,10^{-2}$ (2.00)
$\frac{1}{8}$	$1.59\,10^{-1}$	$7.85\,10^{-2}$ (2.03)	$3.92\,10^{-2}$ (2.00)
$\frac{1}{16}$	$1.38\,10^{-1}$	$6.61\,10^{-2}$ (2.09)	$3.26\,10^{-2}$ (2.03)
$\frac{1}{32}$	$1.08\,10^{-1}$	$4.93\,10^{-2}$ (2.19)	$2.36\,10^{-2}$ (2.09)
$\frac{1}{64}$	$7.92\,10^{-2}$	$3.48\,10^{-2}$ (2.28)	$1.64\,10^{-2}$ (2.12)
$\frac{1}{128}$	$5.69\,10^{-2}$	$2.43\,10^{-2}$ (2.34)	$1.12\,10^{-2}$ (2.17)
$\frac{1}{256}$	$4.06\,10^{-2}$	$1.69\,10^{-2}$ (2.40)	$7.73\,10^{-3}$ (2.19)

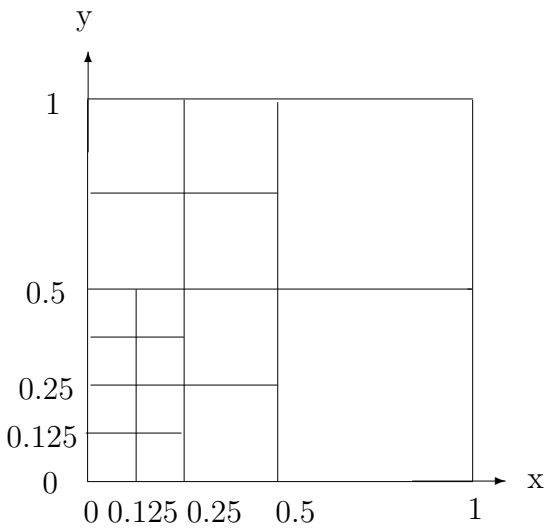

FIG. 2. *Composite grid example.*

of the average value $\frac{\gamma_{\epsilon,N}}{N}$ is refined by quartering. Note that this decision does not separate the roles of u and v, and for this reason alone it is not likely to provide a fully optimal strategy. However, it does produce effective grids for many problems, as the following results suggest.

4.2.1. Example 3: Same as Example 1 with $\epsilon = \frac{1}{32}$. Let $\Omega = [0,1] \times [0,1]$, $\Gamma_D = \partial\Omega$, $\Gamma_N = \emptyset$, $\epsilon = \frac{1}{32}$, $\mathbf{a} = (-1, 0)$, and $g_D = 0$, and define f so that $p(x, y) =$

TABLE 3
$\gamma^{(1)}_{\epsilon,N}$ *and* δ *for composite grids, Example* 3.

Grid level	Bilinear elements for v			Exponential elements for v		
	N	$\gamma^{(1)}_{\epsilon,N}$	δ	N	$\gamma^{(1)}_{\epsilon,N}$	δ
1	4	$1.96\,10^{-1}$		4	$1.72\,10^{-1}$	
2	10	$1.19\,10^{-1}$	1.09	10	$7.47\,10^{-2}$	1.82
3	22	$1.05\,10^{-1}$	0.32	22	$5.48\,10^{-2}$	0.79
4	58	$7.63\,10^{-2}$	0.66	46	$3.58\,10^{-2}$	1.15
5	172	$4.56\,10^{-2}$	0.95	142	$2.02\,10^{-2}$	1.02
6	508	$2.54\,10^{-2}$	1.08	502	$1.03\,10^{-2}$	1.07
7	1606	$1.36\,10^{-2}$	1.09	1744	$5.36\,10^{-3}$	1.05

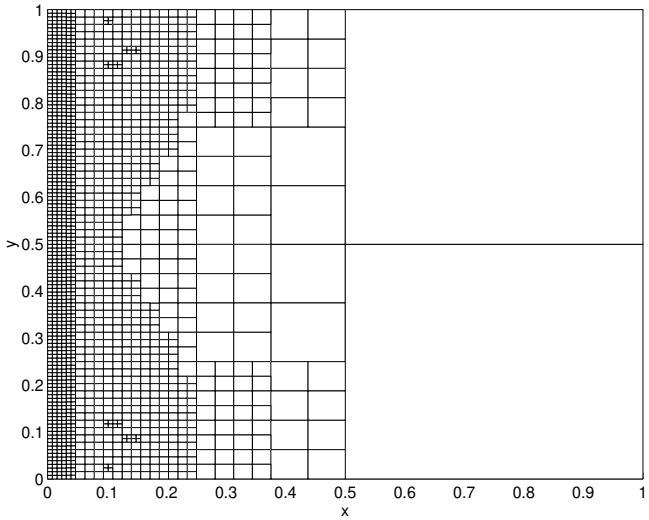

FIG. 3. *Composite grid, Example* 3, *bilinear elements for* v, *level* 7.

$(x-x^2)(y-y^2)e^{-32x}$ solves (1). The fluxes are given by (31) and (32) with $\epsilon = \frac{1}{32}$. Then the exponentially weighted functional involving $\mathbf{u}$ only is

$$G^{(1)}_{\epsilon}(\mathbf{u}; f, \mathbf{0}) = \left\| e^{-16x} u_x + e^{16x} v_y + e^{16x} \frac{1}{\epsilon} f \right\|_0^2 + \left\| e^{-16x} u_y - e^{16x} v_x \right\|_0^2 .$$

Table 3 shows our results for the composite grids with local refinement determined by the strategy described above. Bilinear element are used for u, and both bilinear and exponential elements are used for v. Figures 3 and 4 depict the composite grid for the seventh level for these respective cases. Note that the grids differ because different partition functionals are used. Table 3 shows the results of these tests in terms of N (the number of elements in the composite grid), $\gamma^{(1)}_{\epsilon,N}$, and an estimate of the convergence "order" δ in (29) (computed by comparing $\gamma^{(1)}_{\epsilon,N}$ with its value for the previous N). Note the superiority of using exponential elements and the $\mathcal{O}(h)$-analogous behavior of its error.

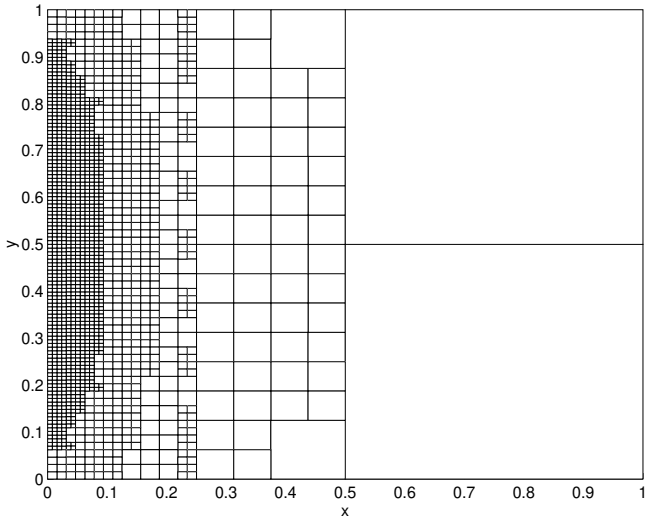

FIG. 4. *Composite grid, Example* 3*, exponential elements for* v*, level* 7.

4.2.2. Example 4: Nonaligned flow and constant coefficients. Let $\Omega = [0,1] \times [0,1]$, $\Gamma_D = \partial\Omega$, $\Gamma_N = \emptyset$, $\epsilon = \frac{1}{32}$, $\mathbf{a} = (-\frac{\sqrt{2}}{2}, -\frac{\sqrt{2}}{2})$, and $g_D = 0$, and define f so that $p(x,y) = (x - x^2)(y - y^2)e^{-16\sqrt{2}(x+y)}$ solves (1). The fluxes are now

$$u = (1 - (2 + 16\sqrt{2})x + 16\sqrt{2}x^2)(y - y^2)e^{-16\sqrt{2}y} \tag{36}$$

and

$$v = (x - x^2)(1 - (2 + 16\sqrt{2})y + 16\sqrt{2}y^2)e^{-16\sqrt{2}x}. \tag{37}$$

Then the exponentially weighted functional involving $\mathbf{u}$ only is

$$G_\epsilon^{(1)}(\mathbf{u}; f, \mathbf{0}) = \left\| e^{8\sqrt{2}(-x+y)}u_x + e^{8\sqrt{2}(x-y)}v_y + e^{8\sqrt{2}(-x-y)}\frac{1}{\epsilon}f \right\|_0^2 + \|e^{8\sqrt{2}(-x+y)}u_y - e^{8\sqrt{2}(x-y)}v_x\|_0^2.$$

The grids we obtained for this example are displayed in Figures 5 and 6. The results are very similar to those of Example 3, as Table 4 shows.

4.2.3. Example 5: Same as Example 2 with $\boldsymbol{\epsilon = \frac{1}{32}}$. Let $\Omega = [0,1] \times [0,1]$, $\Gamma_D = \partial\Omega$, $\Gamma_N = \emptyset$, $\epsilon = \frac{1}{32}$, $\mathbf{a} = (x, -y)$, and $g_D = xe^{\frac{x^2-1}{2\epsilon}} + (1-y)e^{-\frac{y^2}{2\epsilon}}$, and define f so that $p(x,y) = xe^{\frac{x^2-1}{2\epsilon}} + (1-y)e^{-\frac{y^2}{2\epsilon}}$ solves (1). Then $u = 1 + 32x^2$ and $v = -1 - 32y + 32y^2$, and the exponentially weighted functional involving $\mathbf{u}$ only is

$$G_\epsilon^{(1)}(\mathbf{u}; f, \mathbf{0}) = \|e^{8(x^2-1+y^2)}u_x + e^{-8(x^2-1+y^2)}v_y + e^{-8(x^2-1-y^2)}\frac{1}{\epsilon}f\|_0^2 + \|e^{8(x^2-1+y^2)}u_y - e^{-8(x^2-1+y^2)}v_x\|_0^2.$$

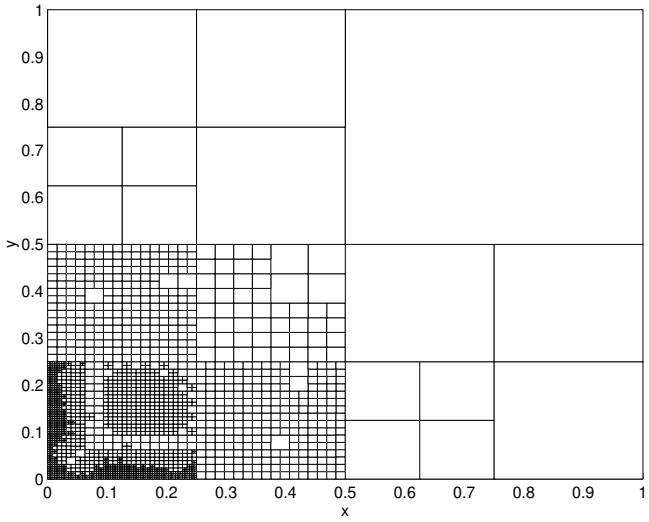

FIG. 5. *Composite grid, Example* 4*, bilinear elements for* $\mathbf{u}$*, level* 8.

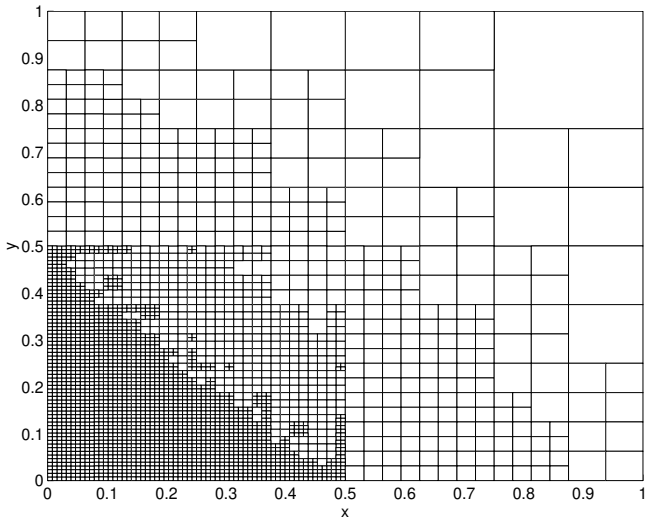

FIG. 6. *Composite grid, Example* 4*, exponential elements for* $\mathbf{u}$*, level* 7.

The full functional involving $\mathbf{u}$ and p is

$$\begin{aligned} G_\epsilon(\mathbf{u},p;f,\mathbf{0}) &= \|e^{8(x^2-1+y^2)}u - e^{-8(x^2-1-y^2)}p_x\|_0^2 \\ &+ \|e^{-8(x^2-1+y^2)}v - e^{-8(x^2-1-y^2)}p_y\|_0^2 \\ &+ \|e^{8(x^2-1+y^2)}u_x + e^{-8(x^2-1+y^2)}v_y + e^{-8(x^2-1-y^2)}\frac{1}{\epsilon}f\|_0^2 \\ &+ \|e^{8(x^2-1+y^2)}u_y - e^{-8(x^2-1+y^2)}v_x\|_0^2. \end{aligned}$$

Bilinear element are used for u, v, and p. Figures 7 and 8 show that the composite grid at the seventh level for the functional $G_\epsilon^{(1)}$ and G_ϵ are not very different, suggesting that the principal task of minimizing G_ϵ is in minimizing the first stage $G_\epsilon^{(1)}$. (It may

TABLE 4
$\gamma^{(1)}_{\epsilon,N}$ *and* δ *for composite grids, Example* 4.

Grid level	Bilinear elements for $\mathbf{u}$			Exponential elements for $\mathbf{u}$		
	N	$\gamma^{(1)}_{\epsilon,N}$	δ	N	$\gamma^{(1)}_{\epsilon,N}$	δ
1	4	1.00		4	$2.36\,10^{-1}$	
2	7	$9.80\,10^{-1}$	0.07	7	$1.50\,10^{-1}$	1.62
3	10	$7.50\,10^{-1}$	1.50	19	$9.08\,10^{-2}$	1.01
4	22	$4.78\,10^{-1}$	1.14	70	$4.93\,10^{-2}$	0.94
5	67	$2.95\,10^{-1}$	0.87	232	$2.47\,10^{-2}$	1.15
6	196	$1.59\,10^{-1}$	1.15	793	$1.26\,10^{-2}$	1.10
7	598	$8.38\,10^{-2}$	1.15	2878	$6.39\,10^{-3}$	1.05
8	1996	$4.61\,10^{-2}$	0.99			

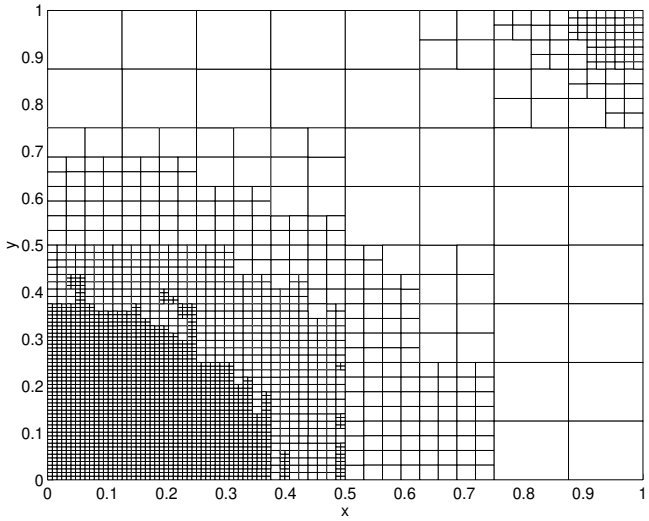

FIG. 7. *Composite grid, Example* 5, $G^{(1)}_{\epsilon}$, *level* 7.

not seem apparent at first glance, but the refinement pattern exhibited in these grids is consistent with the coupled approximation of the individually scaled flux components.) The results are again similar to those of Example 3, with G_ϵ somewhat better than $G^{(1)}_{\epsilon}$, as Table 5 shows. The final approximations are depicted in Figures 9–11 (p_x and p_y are recovered from u and v, respectively).

4.3. Multigrid solvers. One of our objectives in developing the exponentially weighted least-squares functional was to obtain discrete problems that are easily solved by simple multigrid algorithms [4]. Here we report on a representative example of asymptotic multigrid convergence factors for G_ϵ on uniform rectangular grids, with constant $\mathbf{a} = (\cos\theta, \sin\theta)$, zero data ($f = 0$, $\mathbf{g} = \mathbf{0}$), and various ϵ. The problem for this example is the homogeneous equation

$$\begin{cases} -\epsilon\Delta p + \cos\theta p_x + \sin\theta p_y &= 0 \quad \text{in } \Omega, \\ p &= 0 \quad \text{on } \partial\Omega, \end{cases}$$

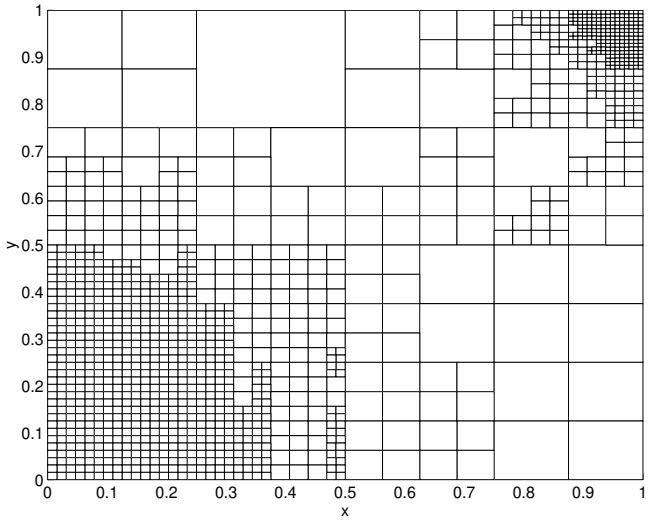

FIG. 8. *Composite grid, Example* 5, G_ϵ, *level* 7.

TABLE 5
Γ_N *and* δ *for composite grids, Example* 5.

Grid level	Functional $G_\epsilon^{(1)}$			Functional G_ϵ		
	N	$\gamma_{\epsilon,N}^{(1)}$	δ	N	$\gamma_{\epsilon,N}^{(1)}$	δ
1	4	$3.34\,10^{-1}$		4	6.12	
2	7	$1.94\,10^{-1}$	1.94	7	1.06	6.27
3	19	$1.11\,10^{-1}$	1.12	16	$3.49\,10^{-1}$	2.69
4	67	$5.30\,10^{-2}$	1.17	37	$1.96\,10^{-1}$	1.38
5	217	$2.70\,10^{-2}$	1.15	130	$8.37\,10^{-2}$	1.35
6	739	$1.40\,10^{-2}$	1.07	367	$4.26\,10^{-2}$	1.30
7	2770	$7.06\,10^{-3}$	1.04	1213	$2.16\,10^{-2}$	1.14

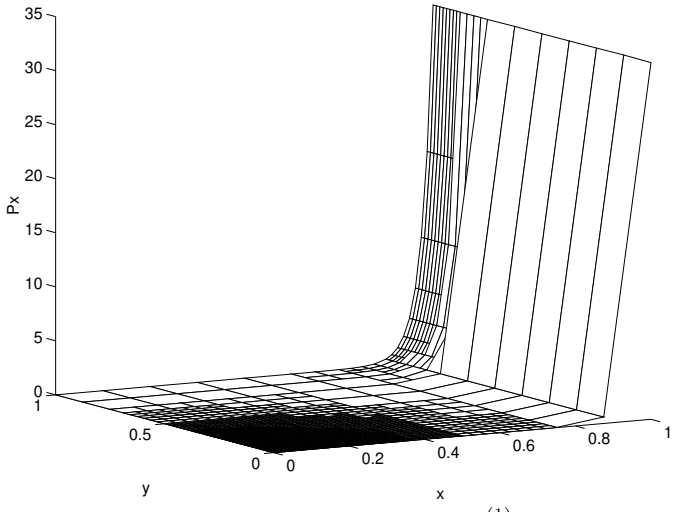

FIG. 9. *Composite grid, Example* 5, $G_\epsilon^{(1)}$, p_x *plot.*

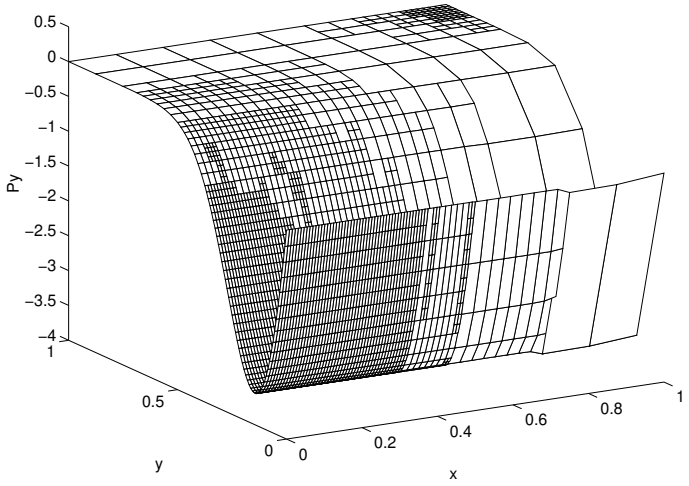

FIG. 10. *Composite grid, Example* 5, $G_\epsilon^{(1)}$, p_y *plot.*

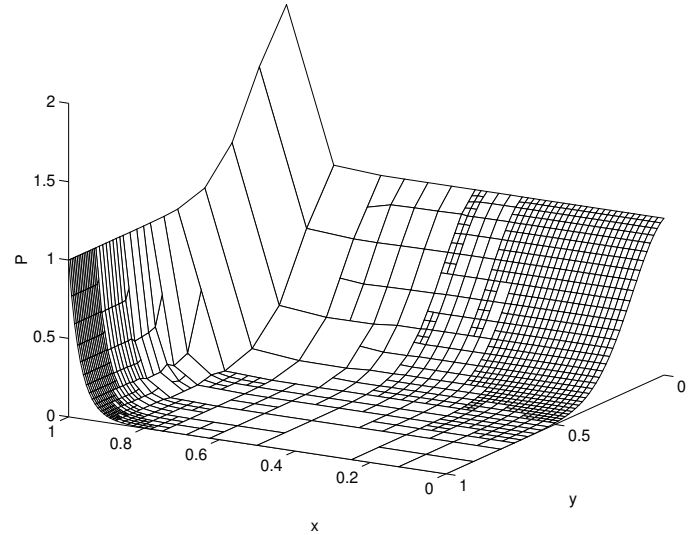

FIG. 11. *Composite grid, Example* 5, G_ϵ, p *plot.*

with the associated functional

$$G_\epsilon(\mathbf{u}, p; 0, \mathbf{0}) = \|e^{\frac{ax-by}{2\epsilon}} u - e^{-\frac{ax+by}{2\epsilon}} p_x\|_0^2 + \|e^{\frac{by-ax}{2\epsilon}} v - e^{-\frac{ax+by}{2\epsilon}} p_y\|_0^2 + \|e^{\frac{ax-by}{2\epsilon}} u_x + e^{\frac{by-ax}{2\epsilon}} v_y\|_0^2 + \|e^{\frac{ax-by}{2\epsilon}} u_y - e^{\frac{by-ax}{2\epsilon}} v_x\|_0^2.$$

We use bilinear elements for all variables. Table 6 shows the asymptotic convergence factor for a standard multigrid algorithm: a V(1,1) cycle with Gauss–Seidel pointwise relaxation and bilinear interpolation. The finest grid used 64×64 elements. The factors were obtained by starting the multigrid process with a random initial guess, then observing worst-case ratios of functional values over successive V cycles. Note that these factors are all below 0.25 and actually tend to improve as convection begins to dominate.

TABLE 6
Asymptotic multigrid convergence factors, $V(1,1)$ cycle, Gauss–Seidel relaxation, 64×64 finest grid.

ϵ	$\theta = 0$	$\theta = 15$	$\theta = 30$	$\theta = 45$
0	0.2340	0.2340	0.2340	0.2340
1	0.2361	0.2360	0.2357	0.2353
$\frac{1}{8}$	0.2375	0.2372	0.2369	0.2354
$\frac{1}{16}$	0.2279	0.2293	0.2295	0.2268
$\frac{1}{32}$	0.2076	0.2162	0.2141	0.2096
$\frac{1}{64}$	0.1768	0.2011	0.1929	0.1830
$\frac{1}{128}$	0.1630	0.1861	0.1620	0.1394
$\frac{1}{256}$	0.1737	0.1656	0.1093	0.0773

5. Conclusion. The purpose of this paper was to study numerical properties of a special FOSLS approach to planar linear convection-diffusion equations, the starting point of which was the basic scheme in [5, 6]. Now with convection-dominated regimes in mind, we used an exponential scaling of the first-order system. The aim was to develop a functional whose bilinear part is equivalent to the square of an analogously scaled vector H^1 norm, uniformly in the size of convection. This coercivity and boundedness in an H^1-like product norm would immediately imply uniformly optimal performance of standard finite element discretization schemes and multigrid solvers. Our objective was to study these properties for problems with varying structure (e.g., constant and variable coefficients, aligned and nonaligned flow) and varying character (e.g., smooth and boundary layer solutions). The results seem to confirm typical H^1-like accuracy of the discretization and optimal multigrid convergence uniformly in the size of convection.

REFERENCES

[1] I. BABUŠKA, *The finite element method with Lagrange multipliers*, Numer. Math., 20 (1973).
[2] P. BOCHEV, Z. CAI, T. A. MANTEUFFEL, AND S. F. MCCORMICK, *Analysis of velocity-flux first-order system least-squares principles for Navier-Stokes equations: Part* I, SIAM J. Numer. Anal., 35 (1998), pp. 990–1009.
[3] F. BREZZI, *On existence, uniqueness and approximation of saddle-point problems arising from Lagrange multipliers*, RAIRO Anal. Numér., 2 (1974), pp. 129–151.
[4] W. L. BRIGGS, *A Multigrid Tutorial*, SIAM, Philadelphia, 1987.
[5] Z. CAI, R. D. LAZAROV, T. MANTEUFFEL, AND S. F. MCCORMICK, *First-order system least squares for partial differential equations: Part* I, SIAM J. Numer. Anal., 31 (1994), pp. 1785–1799.
[6] Z. CAI, T. A. MANTEUFFEL, AND S. F. MCCORMICK, *First-order system least squares for partial differential equations: Part* II, SIAM J. Numer. Anal., 34 (1997), pp. 425–454.
[7] Z. CAI, T. A. MANTEUFFEL, AND S. F. MCCORMICK, *First-order system least squares for Stokes equations, with application to linear elasticity*, SIAM J. Numer. Anal., 34 (1997), pp. 1727–1741.
[8] P. G. CIARLET, *The Finite Element Method for Elliptic Problems*, North–Holland, New York, 1978.
[9] V. GIRAULT AND P.–A. RAVIART, *Finite Element Methods for Navier-Stokes Equations*, Springer, Berlin, New York, 1986.
[10] A. F. HEGARTY, E. O'RIORDAN, AND M. STYNES, *A comparison of uniformly convergent difference schemes for two-dimensional convection-diffusion problems*, J. Comput. Phys., 105 (1993), pp. 24–32.
[11] R. HERBIN, *An error estimate for a four point finite volume scheme for the convection-diffusion equation on a triangular mesh*, Numer. Methods Partial Differential Equations, to appear.

[12] C. Johnson, *Numerical Solution of Partial Differential Equations by the Finite Element Method*, Studentlitteratur, Sweden, 1987.
[13] P. Ladyzhenskaya, *The Mathematical Theory of Viscous Incompressible Flows*, Gordon and Breach, London, 1969.
[14] T. A. Manteuffel and J. S. Otto, *On the Uniform Consistency of an Exponentially Upwinded Discretization for Singular Perturbation Problems*, manuscript.
[15] S. F. McCormick, *Multilevel Projection Methods for Partial Differential Equations*, NSF CBMS Regional Conference Series 67, SIAM, Philadelphia, 1992.
[16] J. Nečas, *Les Méthodes Directes en Théorie des Equations Elliptiques*, Masson, 1967.
[17] P. A. Raviart and I. M. Thomas, *A mixed finite element method for second order elliptic problems*, Lecture Notes in Math. 606, Springer-Verlag, Berlin, New York, 1977, pp. 292–315.